A Multi-Sensor Smart Inhaler System for Adherence Monitoring and Aerosol Particle Optimization Using Real-Time Signal

Mahendra Dwi Fahreza
Instrumentation Engineering Department
Vocational Faculty
Institut Teknologi Sepuluh Nopember
Surabaya, Indonesia
mahendrafhrz1202@gmail.com
ORCID: 0009-0001-8809-0957

Ir. Dwi Oktavianto Wahyu Nugroho, S.T., M.T.
Instrumentation Engineering Department
Vocational Faculty
Institut Teknologi Sepuluh Nopember
Surabaya, Indonesia
Oktovianto_2wn@its.ac.id
ORCID: 0000-0002-6781-0732

***Abstract*—This paper describes a multi-sensor smart inhaler system that uses adaptive actuation and real-time monitoring to improve drug delivery efficiency. Six sensing modalities—flow rate, inhalation pressure, ambient humidity, IMU-based orientation, optical particle concentration, and SpO_2—are integrated into the device along with six actuators: a variable nozzle, solenoid valve, heater, dose-display module, vibrator feedback unit, and LED indicator. To capture the dynamic behavior of inhalation events and actuator responses, each component is mathematically modeled and expressed across time, frequency, continuous-time (s-domain), and discrete-time (z-domain) representations. Inhalation patterns and system performance are thoroughly evaluated thanks to a custom graphical interface that displays raw, noisy, and filtered versions of fourteen system signals. Experimental simulations demonstrate that noise considerably affects both sensor and actuator outputs, even though low-order IIR filtering effectively restores signal stability and spectral clarity. The system's capacity to distinguish between stable, disturbed, and corrected signal states is further highlighted by the multi-domain analysis, which provides a clear picture of internal device dynamics. These features show that comprehensive signal modeling can be used as a decision-support layer for inhaler optimization. The paper presents a multi-sensor approach for intelligent inhaler design to support adherence monitoring, aerosol optimization, and embedded control integration for future smart respiratory-care systems.**

***Index Terms*—Smart inhaler, multi-sensor system, aerosol delivery, biomedical signal processing, s-domain modeling, z-domain analysis, IIR filtering, respiratory monitoring, actuator control, embedded health systems.**

I. Introduction

Technical errors when using inhalers are still common and affect the effectiveness of inhalation therapy. Several systematic reviews and recent literature indicate that inhaler misuse is a critical health challenge. Methods for assessing inhaler technique differ among studies. This leads to prevalence reports that show a wide range based on the method used and the population examined. Thus, a clear and data-driven monitoring system is needed to understand inhalation patterns and support efforts to improve compliance and drug delivery quality [1].

Corresponding author: Oktovianto_2wn@its.ac.id

Electronic smart inhalers, which have sensors to track usage and offer feedback, show promise for improving patient compliance and inhalation quality [2]. At the same time, changes in inhaler design, like adjustments to nozzle shape and airflow control, can enhance particle deposition in the lungs. This has been shown through computational fluid dynamics (CFD) simulations on smart inhalers[3]. These findings confirm that smarter systems require multi-sensor measurement capabilities capable of building a comprehensive picture of inhalation dynamics.

Most current inhalers are still only able to monitor one or two factors, like opening detection or inhalation flowrate. No studies combine multiple sensor types such as flow, pressure, humidity, aerosol particles, IMU, and SpO_2 biometrics with adjustable mechanisms like nozzle control, solenoid valve, and aerosol heating modules. Additionally, few studies provide real-time analysis of inhalation signals across different areas, including the time domain, frequency domain, s-domain, and z-domain. This analysis is crucial for creating controls based on fluid dynamics and aerosol atomization methods.

This research helps address this gap by creating a smart inhaler system. It integrates six main sensors: flow, pressure, humidity, aerosol particle count, IMU, and SpO_2. The system also includes six actuators: nozzle variable, nozzle actuator, heater module, mist indicator, vibration feedback unit, and status LED indicator. It uses mathematical models for all subsystems based on fluid mechanics, sensor signal processing, and actuator dynamics. An interactive GUI displays raw, filtered, and noise-corrected signals in different domains. The system features an adaptive algorithm that can adjust the inhaler output based on sensor feedback in real time. This results in more accurate and safer dose control.

II. Related Works

In the realm of adaptable inhalers, the field has transitioned from what was, for the most part, a passive inhaler to inhalers that have the capacity to track behaviors, analyze inhalation technique, and improve drug delivery through aerosol. Studies

have pointed to factors that continue to undermine the delivery of drug therapy, including failure to track adherence, measure flow rates, and gain a sound understanding of the dynamics of the delivered particles. In spite of fragmentation, the state of the art still lacks attempts to fully converge toward a resolution to the problems of inhalation quality and overall device performance predictive of delivery to the targeted site. Informed by these gaps, the subsequent segment attempts to collate the most pertinent literature available on commercially available and smart inhalers, the methodologies that have shaped a vast number of studies to measure inspiratory flow, particle dynamics, and the critical gaps that point to the fragmented state of the art, highlighting the need for harmonized, multi-sensor, multi-actuator technologies.

A. Smart Inhaler Technologies

Contemporary intelligent inhalers frequently utilize Electronic Monitoring Devices (EMD) for monitoring medication adherence. How digital inhaler devices can further improve adherence is discussed in a recent review mapping the evolution of EMD technology [4].The commercial devices Propeller, Hailie, and Respiro have also taken this approach, but most of them still concentrate solely on the adherence aspect without incorporating models for aerosol flow and particle dynamics, and the equivalent of gas for aerosol flow. They have also incorporated models for the gas of the aerosol and for the gas, and the aerosol gas dynamics.

B. Flow Sensing in Inhaler Systems

The impact of the inhalation technique on the patterns of airflow, the solid velocity, the degree of airflow turbulence, and the amount of the drug that gets clinically deposited makes the analysis of airflow patterns an essential component of the analysis. One research designed a flow configuration and a differential pressure sensor that allows the reconstruction of profile flows, based on the time the flows are registered [5]. Several others have pointed out that the efficiencies of aerosol deposits that are directly inhaled are significantly influenced by the variations of airflow during an inhalation, which is becoming a growing dependence of the new generation of inhalers on fast and precise transient flow rate response inhalation sensors [6].

C. Particle Dynamics & Nozzle Studies

When it comes to assessing deposition efficiency, the specifics of the aerosol, such as its constituents and the size of the individual particles, play a pivotal role in that efficiency. Fletcher et al. demonstrated, using computational fluid dynamics, that variations in the design of the nozzle and the length of the channel can influence the distribution of particle size and the turbulence of the flow [3]. In a subsequent study documented the influence of the environmental condition of humidity on the formation of droplets and the stability of the aerosol from portable inhalation devices [7]. All of these studies collectively demonstrate the requirement of nozzle design, control of heat, and modeling of the behavior of the particles, and that these are the mechanistic principles in the design of a portable inhaler.

D. Gap in Current Research Landscape

Research on smart inhalers to date suffers from considerable lack of measurement approaches and sensor integration. Several papers address one of the following measurement systems: adherence measurement using magnetic sensors; measurement of adherence using accelerometers; flow measurement using differential pressure sensors. However, most papers do not address the full set of key interrelated measurements: particle size, environmental conditions, and features of the inspiratory maneuver. Moreover, commercially available systems do not block qualitative inhalation analysis and therefore are not capable of modifying inhalation conditions. This is the reason for the insufficient cross-domain integration to enable previous systems to adequately sup. Point aerosol delivery in real time. Conversely, the system developed in this study aims to fill this niche by combining multi-sensor monitoring and multi-actuator responses. This system records usage and measures flow, pressure, particle dynamics, humidity, device movement, physiological parameters such as SpO_2, and more. It characterizes and analyzes inhalation more holistically. Data in the time, frequency (FFT), s, and z domains are captured and transformed for more complete domain analysis. This system observes and optimizes the process for aerosol delivery. Adaptation to the inhalation parameters is enabled by the control valves, nozzles, and heaters.

III. System Architecture

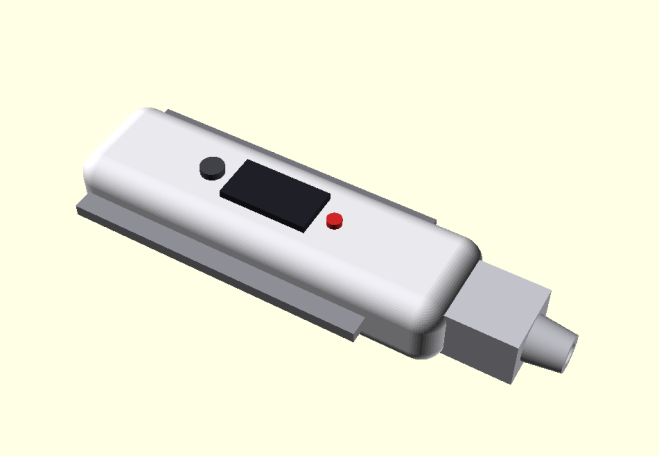

Fig. 1. 3D visualization of the multi-sensor smart inhaler system, showing the geometric structure, nozzle design, and sensor-actuator placement on the device body.

This smart inhaler is designed to interlink six physiological/mechanical sensors and six adaptive actuators to optimize the delivery of aerosols. Each component communicates with a data-embedded processing unit responsible for data collection, signal maintenance, feature separation, inhalation condition prediction, and control of the actuators in real time. The system has also been designed with a multi-function graphical user interface that allows users to visualize and monitor the system's parameters in the time, frequency, and s- and z-domains. Support for these functions is referred to as closed loop control, but in this case the system employs real time control to modulate the position of the nozzle, the activation of

the solenoid and heater, and the use of actuators that provide the user with feedback on system activity.

A. Overall System Diagram

This section summarize the entire system comprising the sensor suite, actuation modules, processing pipeline, and the GUI. The sensors send the unprocessed data to the processing unit, which performs filtering and transforming processes (FFT, Laplace, Z-transform), and proceeds with the conditional analysis (flow threshold, particle density, humidity anomaly, shaking/orientation correctness, drop in SpO_2 analysis). The actuator then controls the aerosol volume, timing, and temperature, and responds to the user. The GUI displays all the statuses in real time

The subsequent illustration represents the system in its entirety. To begin, we demonstrate the model of the system we developed in the current work, which is a multi-sensor based smart inhaler system with a flow, particle, pressure, IMU, humidity, and SpO_2 all stored at the first acquisition site. These sensors offer real-time measurements of the patient's inhalation condition. This data goes to the Processing Core consisting of acquisition, signal filtering, features, analysis, and decision making in order to estimate the condition of the patient. This processing core is the main controller which manages and coordinates the received signals and, in return, provides commands to the actuator

Aerosol delivery is augmented on the output side by the decision engine activating control signals for the actuator modules like variable nozzles, solenoid timing valves, heaters, vibratory feedback, LED indicators, and dose counters. This configuration allows the system to function on a closed-loop basis, where the control module receives inhalation quality information and reacts accordingly. Furthermore, the system is equipped with a GUI Monitor displaying all system information and status, allowing the user to visualize, in real-time, time domain, frequency domain, and the s-domain and z-domain signals. This coalesced system guarantees that the system can operate with responsiveness, accuracy, and adaptability to real-time inhalation scenarios.

B. Sensor Suites

This system uses six types of sensors that work simultaneously to map the dynamics of patient inhalation and aerosol conditions in real time. Each sensor has a different physical basis, and all contribute directly to the developed closed-loop control scheme. The mathematical equations of each sensing mechanism will be explained in Section IV – Mathematical Modeling of Signals, while this subsection focuses on their operational functions and working principles:

1) Flow Sensor: The flow sensor measures the patient's breathing rate profile in real time. It works by using pressure drops in venturi or orifice geometries, so that changes in pressure represent changes in air flow velocity according to Bernoulli's principle [8]. This module acts as the core of the flow-based modulation mechanism, which regulates the intensity of aerosol delivery based on the patient's breathing pattern.

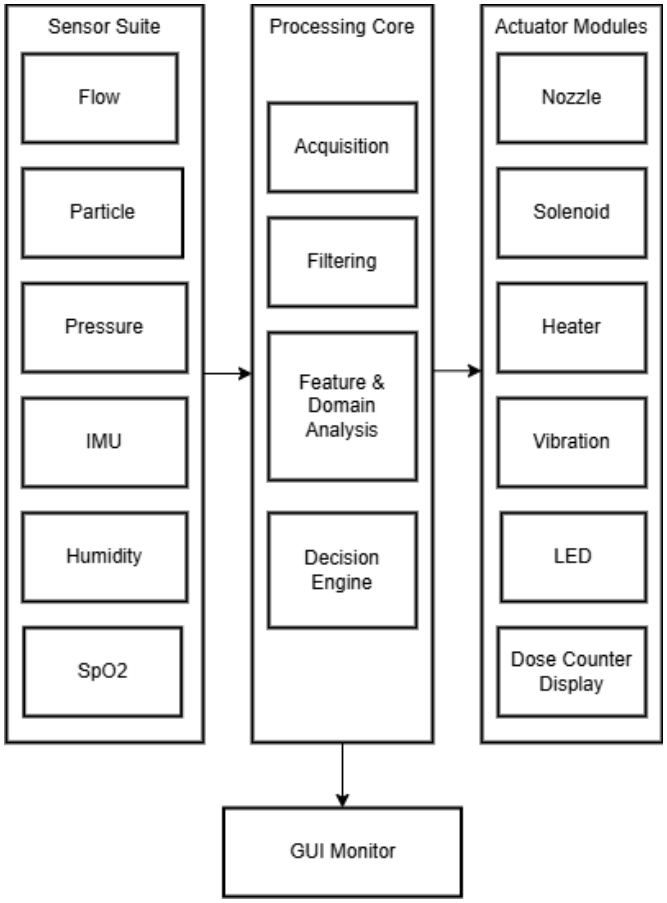

Fig. 2. Overall system architecture of the proposed multi-sensor smart inhaler. The diagram illustrates the integration of the sensor suite, processing core, actuator modules, and real-time monitoring GUI within a unified closed-loop framework.

2) Optical Particle Counter: The working mechanism of the particle sensor is based on counting the photons received from light that is scattered by aerosol particles [9]. As aerosol particles traverse an optical path, the scattering of light changes based on the particles' size, and concentration. These changes of scattering intensity are converted by the photodiode component into electrical signals. This sensor gives real-time estimates of the distribution of particles by size and concentration of the aerosol, which is valuable information for the nozzle actuator.

3) Inhalation Pressure Sensor: The inhalation pressure sensor uses an elastomeric membrane as its sensitive element [10]. When the patient inhales, the suction force deforms the membrane. This change is converted into a shift in capacitance or resistance. This sensor ensures that the inhalation force surpasses the minimum threshold needed for effective drug delivery.

4) Orientation (IMU) Sensor: IMU sensor measures acceleration and orientation for two important functions which detecting shaking before use and ensuring that the inhaler is in a vertical position during actuation or misunderstanding of directions [11]. Changes in the angle of inclination can affect aerosol deposition and pMDI jet momentum. Therefore, this sensor is crucial for maintaining consistent device performance.

5) Ambient Humidity Sensor: Humidity sensors play a key role in inhalers since monitoring humidity is crucial [12]. The humidity sensor measures the RH (Relative Humidity) level at the mouthpiece. It works on the principle that changes in dielectric constant occur with water vapor content. This allows the sensor to identify when the patient exhales into the mouthpiece, indicating that RH is close to 100%. This feature acts as an error detector, as exhalation can harm the aerosol pattern.

6) SpO Sensor: The SpO_2 sensor operates using photoplethysmography (PPG). In this method, red and infrared light is absorbed differently by oxygenated hemoglobin [13]. Changes in absorbance help calculate the patient's oxygen saturation. This measurement is used to check the therapeutic response after a dose is given.

C. Actuator Modules

The actuators in this system are not just static output parts. They play a key role in a control loop that adjusts aerosol and inhalation conditions based on real-time sensor signals. This mix of actuators and controls lets us change physical factors like release time, thermal conditions, and user feedback. This ensures that the drug dose is delivered in the best way to the lungs.

1) Variable Nozzle Actuator: This actuator changes the nozzle opening mechanically, using piezo elements or micro-electromechanical mechanisms. This regulates flow speed and aerosol particle size. Changes in nozzle shape significantly affect particle distribution and the amount of aerosol that can be inhaled. A study shows that the design of the nozzle and actuator greatly influences spray patterns and aerosol features in pMDIs [14].

2) Solenoid Timing Valve: The solenoid valve controls when the aerosol pathway opens, allowing drug delivery to happen at the same time as the patient inhales. The solenoid mechanism allows for quick and precise switching between closed and open states, which reduces overspray and prevents deposition in the oropharynx. Reliable and well-controlled solenoid valve technology is commonly found in automatic inhaler devices in modern research.

3) Heater: The heater keeps the temperature of the aerosol pathway steady. This helps prevent particles from condensing or changing size, which affects aerosol stability. In some aerosol delivery devices, controlling temperature is important for consistent aerosol output, especially in different environmental conditions. Humidity and temperature sensors can provide information to the controller to turn on the heater if conditions suggest possible condensation. This helps keep particle size within the respirable range.

4) Vibratory (Haptic) Feedback: Tactile feedback from vibration signals to the user that inhalation has been done correctly or that the dose has been released. In medicine and human-machine interaction, vibrotactile actuators provide tactile cues for breathing and inhalation procedures. This vibration feedback helps users, especially those who are new or pediatric patients, know when their inhalation is correct, improve their technique, and reduce misuse [15].

5) LED Indicator: LED indicators offer quick visual feedback. They confirm whether inhalation is valid, show when a dose has been delivered, or provide warnings if an error happens, such as insufficient flow or incorrect orientation. Many modern portable medical systems use LED indicators to communicate status in a straightforward way. This visual feedback is helpful for patients and caregivers, ensuring the dose and use of the inhaler are done correctly.

6) Dose Counter Display Actuator: The dose counter module, which uses a digital or OLED display, shows the remaining dose in real time. It updates only when the system detects a valid inhalation. This dose counter connects inhalation validation with dose reduction and has been built into the design of automatic and controlled inhalers. With a validation and actuation loop, this dose counter helps stop wasted doses from misfires. It also offers safer and clearer dose control for users

IV. SIGNAL MODELING FRAMEWORK

Signal modeling is a key part of the proposed multi-sensor smart inhaler system. Each sensing and actuation module produces dynamic responses that need to be represented mathematically, simulated accurately, and analyzed in various domains. The framework created in this study provides a clear method for generating time-varying signals. It also transforms these signals into frequency-domain components and represents their behavior in both continuous-time and discrete-time forms. This modeling structure allows for consistent interpretation of sensor outputs, actuator dynamics, and overall system behavior. It also supports noise injection, filtering methods, and real-time parameter adjustments in the graphical interface. By putting these signal representations into a well-organized processing pipeline, the system lays a strong foundation for analyzing inhalation profiles, aerosol delivery features, and interactions between the device and user across a wide range of operating conditions.

A. Overview of Multi Domain Signal Generation

The development of a multi-sensor smart inhaler needs a clear signal modeling framework that can represent dynamic inhalation behavior and actuator responses in real time. Measuring inhalation flow profiles in real time is essential for smart inhaler systems. These inhalation flow-time curves help the device confirm dose intake and spot improper inhalation techniques that can hurt drug delivery efficiency [16]. Recent advancements in digital inhalers show that pressure-derived inhalation signals can accurately estimate inspiratory parameters like Peak Inspiratory Flow and inhaled volume when analyzed with specific signal extraction algorithms [17]. This accuracy highlights the need to generate continuous time-domain waveforms for each sensor. Time-resolved sampling helps reconstruct inhalation patterns, transient actuator behaviors, and synchronization events between user actions and device mechanics [18].

Beyond time-domain analysis, frequency-domain processing offers additional insights into the performance of sensors and actuators. Frequency decomposition is widely used in digital respiratory monitoring to isolate oscillatory components, detect abnormal breathing issues, and characterize noise patterns that

affect signal interpretation [19]. Continuous-time modeling of actuator components, such as microfluidic nozzles, solenoids, and thermal elements, typically uses dynamic system representations. These representations allow for the analysis of stability, transient response, and control traits under different operating conditions [20]. In embedded biomedical devices, discrete-time digital filtering and signal processing are usually applied to support real-time estimation and control. However, the use of a complete time-domain, frequency-domain, and discrete-time modeling pipeline specific to smart inhalers has not been explicitly documented in published research. Therefore, the z-domain implementation in this study is a methodological contribution of the proposed system.

Integrating multi-domain signal representations into a single framework improves system robustness. It allows for effective filtering, noise suppression, and multi-sensor fusion. Recent research on respiratory monitoring shows that combining different sensor signals with noise-aware filtering greatly boosts estimation accuracy, even with motion artifacts, humidity changes, and user-induced disturbances [21]. This research adopts these principles by modeling each sensor and actuator using its governing equations. It generates their time-domain signals, analyzes their frequency behavior using FFT, and represents their continuous-time and discrete-time characteristics. This establishes a clear signal environment for the inhaler system.

The resulting framework allows for the generation of fourteen different waveforms. These include six raw sensor signals, six actuator outputs, and two composite multi-sensor representations. This setup enables a detailed assessment of inhalation events. This multi-layered signal processing method matches the strategies used in new connected drug delivery devices. These devices increasingly use multiple types of sensors and digital processing to improve adherence monitoring and optimize therapeutic aerosol delivery [4].

B. Mathematical Modeling of Sensor Signals

1) Ambient Humidity Sensor: Ambient humidity in the system is modeled using a capacitive relative humidity (RH) sensor whose output is proportional to the change in capacitance as a function of water vapor content in the air. Capacitive RH sensors are widely used in environmental and respiratory applications due to their good linearity, long-term stability, and fast response to humidity changes. The model used expresses normalized sensitivity S as a function of effective capacitance cp, dry reference capacitance c0, and target humidity φ (in %RH) [22]. This equation below:

$$S = \frac{c_p - c_0}{100\varphi} \tag{1}$$

In the SHT3x sensor-based digital implementation, the RH value is reconstructed from the 16-bit SRH ADC output using the linear relationship from the datasheet:

$$RH = 100 \cdot \frac{S_{RH}}{2^{16} - 1} \tag{2}$$

In the GUI code, φ is set via a slider (20–80 %RHP, cp is sinusoidally modulated to simulate humidity variations in the mouthpiece, then entered into the S formula and finally converted to RH as above.

2) SpO_2 Sensor: SpO_2 users are modeled based on the standard principles of photoplethysmography (PPG) pulse oximetry. This method uses the ratio of ratios between the AC and DC components of the red and infrared signals. Several studies on pulse oximetry explain that this ratio is the key variable calibrated against arterial oxygen saturation [23]. The optical ratio R is written as:

$$R = \frac{\frac{AC_{red}}{DC_{red}}}{\frac{AC_{IR}}{DC_{IR}}} \tag{3}$$

where AC red and AC IR are the pulsatile (AC) components of the red and infrared PPG signals, while DC red and DC IR are their constant (DC) components. This equation is identical to the standard form of ratio modulation used in commercial pulse-oximetry systems. In the GUI code,

3) Inhalation Pressure Sensor: The inhalation pressure sensor models the differential pressure generated by inspiratory flow through the mouthpiece. In smart inhaler systems, ΔP measurements are often used to reconstruct the inhalation flow rate profile and evaluate the patient's suction resistance [24]. The model used in this system is a raw pressure signal p[t] generated as an offset sinusoid with an amplitude of pAmp. Then adaptive peak tracking is performed to obtain the highest peak value vhigh[t] through an exponential filter with two decay coefficients α_A (rising edge) and α_R (falling edge):

$$v_{high}[t] = \begin{cases} \alpha_A v_{high}[t-1] + (1-\alpha_A)p[t], & \text{jika } p[t] \geq v_{high}[t-1], \\ \alpha_R v_{high}[t-1] + (1-\alpha_R)p[t], & \text{jika } p[t] < v_{high}[t-1]. \end{cases} \tag{4}$$

Digital differential sensors such as the Sensirion SDP3x produce an integer output of S ticks which is converted to physical pressure via a scale factor datasheet.

$$\Delta P = \frac{S_{ticks}}{S_{scale\_factor}} \tag{5}$$

In GUI, S ticks are approximated by v high [t], so that ΔP follows adaptive dynamics that resemble the patient's peak suction pressure during the inhalation maneuver.

4) Orientation (IMU) Sensor: The orientation sensor is modeled as an IMU (accelerometer + gyroscope) that provides measured acceleration $\tilde{a}(t)$ and measured angular velocity $\tilde{\omega}(t)$. The general IMU model includes the effects of rotation, bias, and stochastic noise:

$$\tilde{a}(t) = R^T(t)(a(t) - w_g) + b^a(t) + \eta^a(t) \tag{6}$$

$$\tilde{\omega}(t) = \omega(t) + b^g(t) + \eta^g(t) \tag{7}$$

where R(t) is the rotation matrix, wg is the gravity vector, ba and bg are the accelerometer and gyroscope biases, and ηa and ηg are the noise components [25]. In the GUI, this model is simplified to a single acceleration axis ax(t) derived from the tilt angle $\theta(t)$:

$$\theta(t) = \theta_m a_x \sin(2\pi f t), \qquad a_x(t) = g\sin(\theta(t)) \tag{8}$$

then added bax bias and random noise:

$$\tilde{a}_x(t) = a_x(t) + b_{(ax)} + \eta_a(t) \tag{9}$$

5) Particle Optical Counter Sensor: The particle counter used is a laser-scatter-based optical particle counter (OPC). It measures how much light is scattered when particles pass through a narrow beam. The OPC sorts particles into different size channels based on the level of the detected light pulse. It also counts the number of particles in each channel to estimate particle size distribution and concentration [26].

The model used expresses the total aerosol mass concentration Cm as:

$$C_m = K \sum (i = 1)^n N(v_i) v_i^{1.5} \tag{10}$$

6) Flow Sensor: The flow sensor measures the volumetric flow rate Q of air through the mouthpiece using Bernoulli's equation for orifice flow. Many smart inhalers and differential pressure-based spirometry systems depend on the connection between ΔP and Q in the flow restriction element [27]. The models used are:

$$Q = C_d A_c \sqrt{\frac{2\Delta P}{\rho}} \tag{11}$$

where Cd is the discharge coefficient, Ac is the cross-sectional area, ΔP is the pressure difference from the previous pressure sensor (Sensirion SFM3000), and ρ is the air density. In the GUI, Cd is set by a slider, Ac is set to $1 \times 10^{-4}\,\mathrm{m}^2$, and ΔP is taken from the pressure sensor output.

C. Mathematical Modeling of Actuator Signals

1) Variable Nozzle Actuator: Variable nozzle actuation is modeled as a first-order dynamic system driven by the inhalation flow signal. Research on compliant micro-nozzle and flow-adaptive actuation shows that variable geometry elements can be described using a linear time-invariant (LTI) first-order differential model. This model has a response time constant τ_s and a damping coefficient ρ_s which allow for smooth mechanical convergence to a commanded flow-dependent state [28]. The governing equation that describes the nozzle displacement response $\bar{y}$ to the input excitation $\bar{x}$ is expressed as:

$$\bar{y} = \frac{1}{\tau_s s + \rho_s} \bar{x} \tag{12}$$

This continuous-time system maps inhalation-driven modulation into a smoothed control surface motion, aligning with first-order actuator models in adaptive microfluidic nozzles.

2) Valve Timing Solenoid: Solenoid actuation controls the timing of airflow in inhaler systems. Based on electromagnetic actuator modeling, the force produced relates to the change in magnetic co-energy λ concerning plunger position x_p, adjusted by coil current $i(t)$ [29]. The force model is:

$$F = \frac{\partial \lambda(x_p, i)}{\partial x_p}\, i \tag{13}$$

3) Vibratory Feedback Actuator: The vibratory actuator gives haptic feedback to help users inhale correctly. Research on tactile biofeedback actuators describes their output displacement as a Gaussian-modulated vibration envelope [29]. This envelope shows resonance behavior around a central mechanical state. The output of the actuator is represented as:

$$y = e^{-k - m^2 g \cdot \sigma^2} \tag{14}$$

where m is the center resonance parameter, k is the instantaneous stiffness modulation, and $(g + \sigma^2)$ controls the width of the Gaussian activation region. This formulation produces a smooth tactile vibration with amplitude dependent on real-time modulation.

4) Dose Counter Display Actuator: Digital dose counters usually show a luminance decay pattern. This pattern can be modeled with a stretched exponential function, which is common in modeling luminance degradation in OLED and thin-film displays [30]. The evolution of display luminance is:

$$L_t = L_0 \exp\left(-\frac{t}{\tau^\beta}\right) \tag{15}$$

where L_0 is the initial luminance, τ is the characteristic decay time, and β is the stretch exponent. We include small harmonic oscillations and random noise in the simulation to mimic realistic visual flicker and sensor or display variability.

5) Heater: The heater is designed based on the thermal conductivity rules for multilayer thin-film heating structures. Effective conductivity σ_{tot} is defined as the thickness-weighted combination of oxide and nitride layers [31]. The model used is:

$$\sigma_{tot} = \frac{t_{ox}\sigma_{ox} + t_{nit}\sigma_{nit}}{t_{ox} + t_{nit}} \tag{16}$$

where t_{ox} and t_{nit} are the layer thicknesses, and σ_{ox} and σ_{nit} are the corresponding thermal conductivities. During dynamic operation, heater output is adjusted with sinusoidal thermal fluctuation to mimic pulsatile heating behavior.

6) LED Indicator: LED radiation intensity follows the classical semiconductor diode equation. Here, the radiative current I_{rad} is exponentially related to the junction voltage V_j [32]. This relationship is well-supported in modeling LED electro-optical devices:

$$I_{rad} = I_{rad,0} \exp\left(\frac{qV_j}{n_{ideal,R} kT}\right) - 1 \tag{17}$$

where I_0 is the reverse saturation current, q is the electron charge, n is the ideality factor, k is the Boltzmann constant, and T is temperature. The LED output in simulation converts this current into milliampere level for visualization.

D. Noise Modelling

Noise is added to each of the twelve sensor and actuator signals to mimic realistic measurement disturbances caused by airflow turbulence, mechanical vibration, electronic quantization, and changes in the environment [33]. In the simulation, a uniformly distributed noise term is applied to every signal

to represent random fluctuations without bias. For each signal $x(t)$, the noisy version $x_n(t)$ is generated as:

$$x_n(t) = x(t) + \eta(t) \tag{18}$$

where $\eta(t)$ is a zero-mean random disturbance defined as:

$$\eta(t) = A_n(2r - 1) \tag{19}$$

with $r \in [0, 1]$ as a uniform random variable and A_n as the noise amplitude, which is set to 0.4 for all signals. This approach simulates broad disturbances that frequently occur in multi-sensor inhalation monitoring systems. The noise term is applied the same way in the Raw, Noisy, and Filtered domains to keep temporal consistency during visualization and analysis.

E. Filtering and Signal Reconstruction

To stabilize the noisy signals and adjust sensor conditioning circuits, a first-order infinite impulse response (IIR) low-pass filter is applied to each signal [34]. This filter smooths the injected noise and provides a stable filtered output $x_f(t)$. The recursive filter is defined as:

$$x_f[n] = x_f[n-1] + \alpha\left(x_n[n] - x_f[n-1]\right) \tag{20}$$

where α is the smoothing coefficient ($\alpha = 0.02$). This represents the discrete-time approximation of a continuous-time first-order system with a time constant $\tau \approx \Delta t/\alpha$. The filter effectively removes high-frequency disturbances from the Noisy domain while keeping the temporal dynamics in the Raw signal. This low-pass filtering step also helps maintain the stability of future FFT computation and combined-domain visualization.

F. Frequency-Domain Representation (FFT Computation)

Frequency-domain analysis offers a crucial view of how inhalation signals and actuator responses behave over time. It helps identify key oscillatory components, mechanical resonances, and noise-related artifacts. Fourier-based spectral analysis is commonly used in biomedical sensing systems to extract patterns from physiological signals, including respiratory flow, photoplethysmography (PPG), and airflow-modulated measurements. In particular, using FFT for estimating respiration rates from PPG signals has proven effective for real-time respiratory monitoring. This shows the importance of spectral decomposition in health-related sensor systems [35].

Each signal is changed into the frequency domain using a discrete Fourier transform (DFT) implementation that computes magnitude spectra over a fixed window of $N = 128$ samples. The magnitude of the k-th spectral component $X[k]$ is calculated as:

$$\mathrm{Re}[k] = \sum_{t=0}^{N-1} x[t] \cos\left(\frac{2\pi k t}{N}\right) \tag{21}$$

with

$$\mathrm{Im}[k] = -\sum_{t=0}^{N-1} x[t] \sin\left(\frac{2\pi k t}{N}\right) \tag{22}$$

$$X[k] = \frac{\sqrt{\mathrm{Re}[k]^2 + \mathrm{Im}[k]^2}}{N} \tag{23}$$

Only the first half of the spectrum ($N/2$ bins) is retained to represent frequencies in the range $[0, f_s/2]$, where $f_s = 1/\Delta t = 20$ Hz. The magnitude is normalized relative to the maximum spectral amplitude in each frame:

$$X[k] = \frac{X[k]}{\max(X[k])} \tag{24}$$

This FFT framework enables identification of characteristic inhalation frequencies, actuator resonance patterns, and dynamic coupling between sensor and actuator behaviors.

G. Combined System Response in the s-Domain

To get a single view of the system's global dynamic state, the framework creates a combined signal that represents the average instantaneous amplitude across the twelve sensor and actuator channels. The combined time-domain signal $c(t)$ is computed as:

$$c(t) = \frac{1}{N_s} \sum_{i=1}^{N_s} s_i(t) \tag{25}$$

where $N_s = 12$ is the total number of signals. For stability and consistent visualization in the s-domain, $c(t)$ is normalized:

$$c(t) = \frac{c(t) - \min(c(t))}{\max(c(t)) - \min(c(t))} \tag{26}$$

H. Combined System Response in the z-Domain

The discrete-time representation of the combined multi-sensor and multi-actuator signal is further analyzed in the z-domain. Given the normalized combined signal $c(t)$ sampled at intervals of T_s, the discrete-time sequence is:

$$c[n] = c(nT_s) \tag{27}$$

The z-transform is then:

$$C(z) = \sum_{n=0}^{N-1} c[n] z^{-n} \tag{28}$$

To visualize discrete-time behavior without computing a transfer function, a pole-zero-like distribution is created by projecting FFT magnitudes onto the complex unit circle:

$$r_k = r_{\min} + (r_{\max} - r_{\min}) \frac{M_k}{\max(M)} \tag{29}$$

$$z_k = r_k e^{j\theta_k} \tag{30}$$

where M_k is the FFT magnitude at bin k, and $\theta_k = \frac{2\pi k}{N/2}$ is the angular location. $r_{\min} = 0.2$ and $r_{\max} = 1.0$ define the stable visualization bounds.

Points with large spectral magnitude ($M_k > 0.7 \max M$) are sometimes shown as "pseudo-poles." This gives helpful insight into resonance-like behavior or stimulus-driven actuator and sensor synchrony. Such a z-domain projection allows the

system to show global discrete-time interactions caused by simultaneous changes in inhalation flow, pressure modulation, vibratory feedback, solenoid actuation, and LED current variations. Similar pole and zero visual mapping techniques have been used in digital biomedical instruments to detect oscillatory patterns, periodic biomechanical events, and instabilities in wearable or respiratory monitoring systems.

V. Result

As an overview of the implemented system, the complete graphical user interface (GUI) used for real-time monitoring and signal visualization is shown in Fig 3.

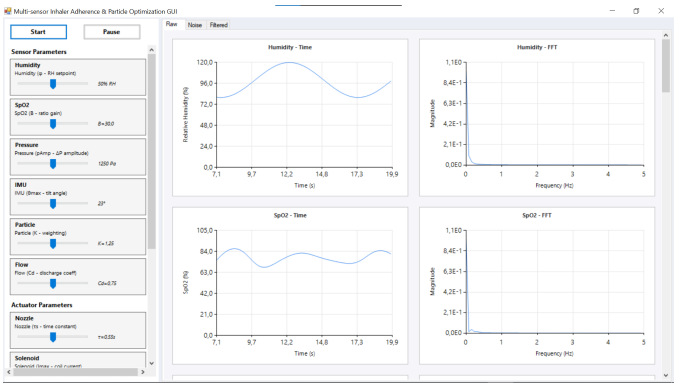

Fig. 3. Overview of the developed multi-sensor inhaler adherence and aerosol optimization GUI showing time-domain and frequency-domain visualization panels.

A. Raw Signal Characterization

Direct, unfiltered results of all sensor and actuator models, therefore reflecting their natural physical or mathematical behavior, the raw signals produced by the system represent the direct, unprocessed outputs. These raw waveforms exhibit distinct periodicity in the time domain derived from the sinusoidal inhalation-driven changes in the sensing modules and the deterministic dynamic reactions recorded in the actuator models. The crude frequency-domain spectra further support this behavior as most channels show a powerful fundamental component inside the low-frequency band related with inhalation cycles, actuator modulation, and slow biomechanical oscillations often seen in respiratory monitoring systems. Appearing small and highly structured in the raw state, the combined s-domain representation combines all sensor and actuator channels onto one pole–zero map. While sensor-related zeros line along the imaginary axis, showing steady, noise-free continuous-time behavior over the whole multi-signal system, Poles linked with first-order actuator dynamics remain grouped along the negative real axis.

In the IMU, the raw acceleration signal displays a smooth sinusoidal path mirroring the simulated inhalation-induced tilted movement. While its FFT spectrum reveals a clearly defined peak close to its modulation frequency and the lack of broadband elevation validates a noise-free measuring environment. IMU contribution to the s-domain pole–zero chart runs nearly on the imaginary axis. This makes the IMU signal

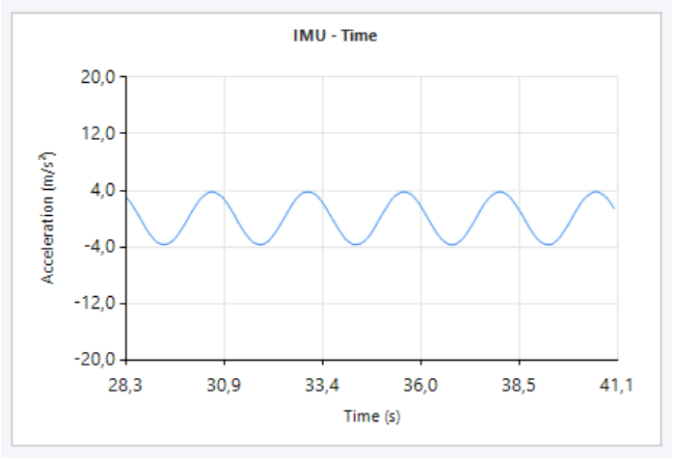

Fig. 4. IMU – Time Domain Raw Signal

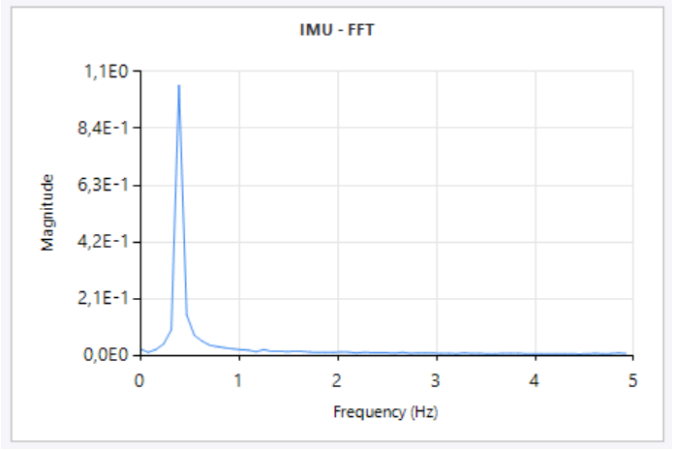

Fig. 5. IMU – FFT Spectrum Raw Signal

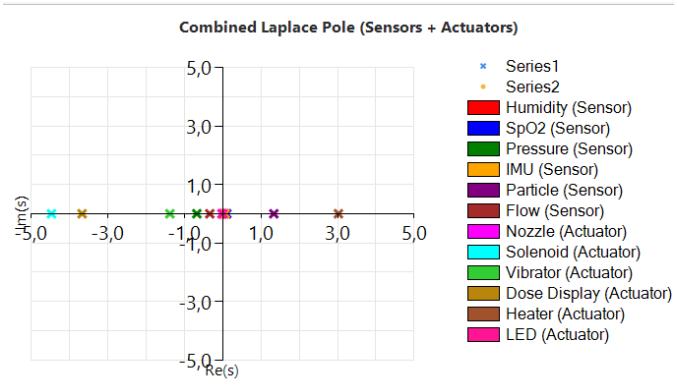

Fig. 6. s Domain Mapping Raw Signal

an excellent representative example for demonstrating the multi-domain raw signal behavior described in this segment. The IMU acceleration signal is used for the raw multi-domain visualizations presented in the figures accompanying this section.

B. Noise Influence and Distortion Analysis

Noise injection generates disturbances that impact the spectral distribution as well as the amplitude of all sensor

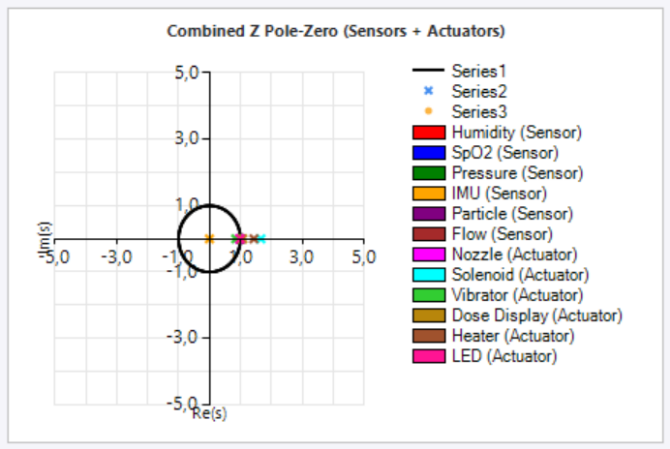

Fig. 7. z Domain Mapping Raw Signal

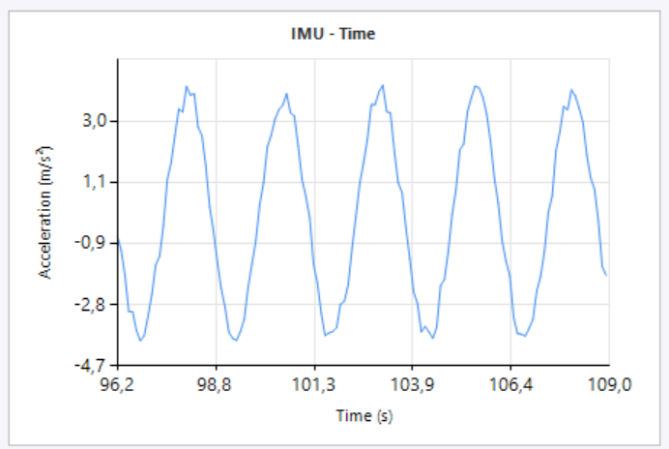

Fig. 8. IMU – Time Domain Noise Added Signal

and actuator signals. High-frequency variations disrupt the periodic patterns and obscure the natural dynamics of the underlying physical models in the time domain. Consistent with the behavior of noisy biological and inertial biosignals affected by motion artefacts, turbulence, or electronic interference, the spectral representation reflects this degradation via broadband elevation and decreasing contrast between the major modulation frequency and its adjacent components. In the s-domain representation noise shows up as a more extensive and less arranged pole–zero distribution. Less coherent dynamic signature results from actuator poles moving from their nominal locations and zeros representing sensor channels spreading more broadly across the complex plane than in the raw condition. This dispersed pattern shows how noise pollution causes the multi-sensor inhaler system to lose stability and synchrony.

For the IMU in particular, noise causes erratic accelerometer oscillations that obscure the pure oscillatory motion visible in the raw signal. Its FFT spectrum shows high broadband elements, so obscuring the fundamental frequency. In the combined s-domain visualization, the IMU-associated zeros scatter into a bigger area, indicating more dynamic variability and less coherence within the inertial subsystem. These alterations show the IMU as an excellent example of how multi-domain features throughout the inhaler's sensing architecture are impacted by noise.

C. Filter Performance Evaluation

The low-order IIR filtering level application significantly enhances the sensor and actuator signal overall quality across every channel. Filters in the time domain stifle high-frequency artefacts while yet preserving the basic oscillatory behaviour linked with inhalation and actuator dynamics. Similarly, the frequency-domain spectra recover clearly defined peaks and broadband noise parts are much reduced, hence creating a cleaner and more physiologically relevant representation. This change is also seen in the s-domain visualization: the pole-zero distribution shrinks back toward the stable and ordered arrangement seen under raw circumstances. Following the filtering process, actuator poles realign along the negative real axis while sensor zeros return to a smaller area near the

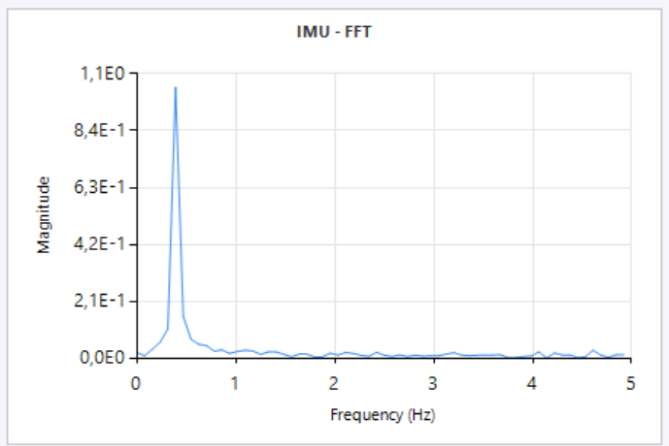

Fig. 9. IMU – FFT Spectrum Noise Added Signal

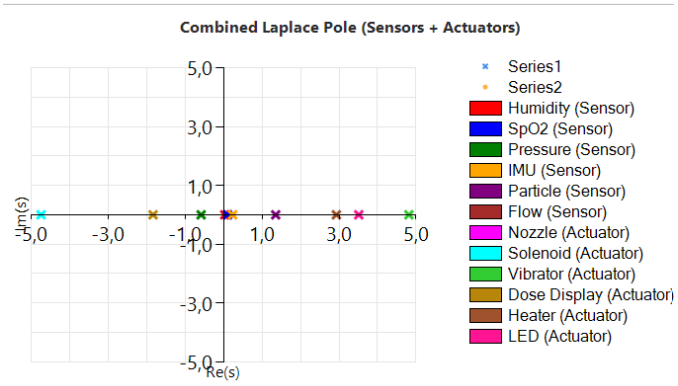

Fig. 10. s Domain Mapping Noise Added Signal

imaginary axis, hence implying regained system stability and coherency.

The filtering process on the IMU channel brings back the smooth sinusoidal acceleration profile defining the planned inhalation-induced movement. With the noise floor much lowered, its FFT spectrum becomes once more sharply peaked. Reflecting a re-stabilized dynamic structure consistent with the initial system behavior, in the s-domain map the IMU zeros converge toward the imaginary axis.

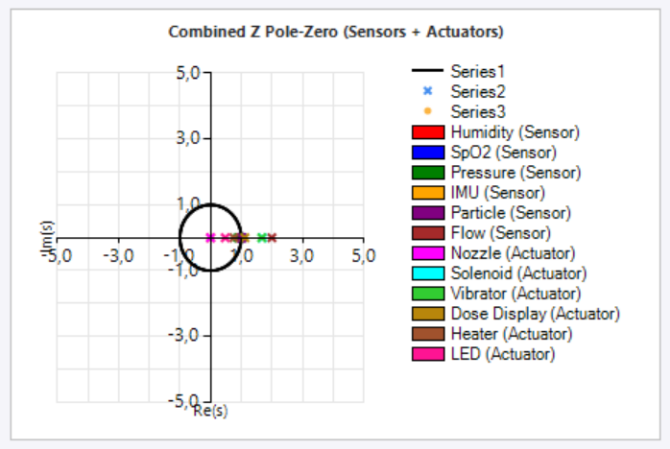

Fig. 11. z Domain Mapping Noise Added Signal

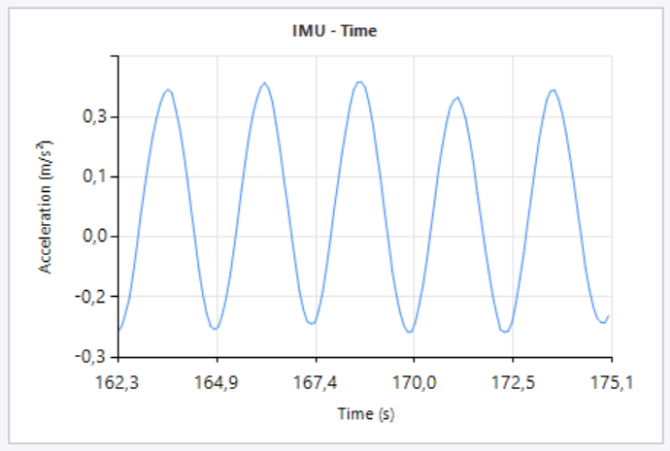

Fig. 12. IMU – Time Domain Filtered Signal

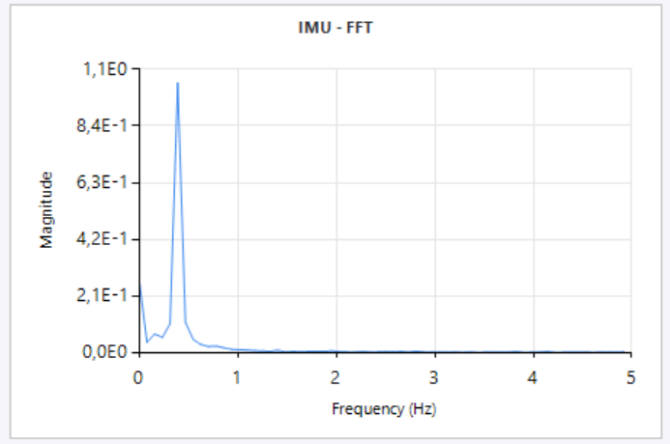

Fig. 13. IMU – FFT Spectrum Filtered Signal

VI. Conclusion

The creation of a comprehensive multi-sensor smart inhaler capable of tracking inhalation behavior, measuring aerosol-related physical characteristics, and modulating actuator responses in real time was presented in this study. The system effectively establishes a unified closed-loop framework for maximizing drug delivery efficiency by integrating six heterogeneous sensors—flow, pressure, humidity, IMU, particle counter, and SpO_2—with six coordinated actuators. A complete mathematical modeling architecture was implemented to represent each sensor and actuator in the time domain, frequency domain, continuous-time s-domain, and discrete-time z-domain, enabling transparent interpretation of device dynamics and user interaction patterns.

Fourteen different waveforms, comprising raw, noisy, and

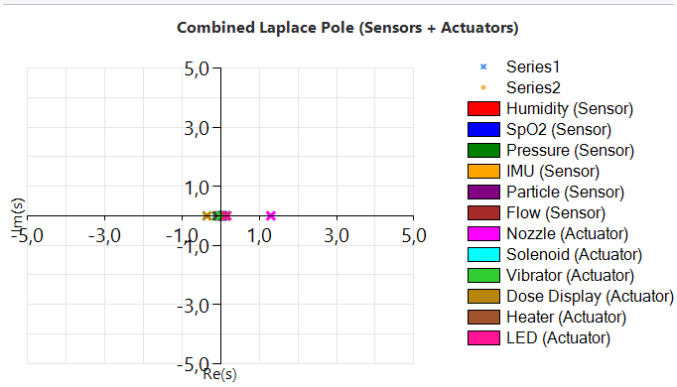

Fig. 14. s Domain Mapping Filtered Signal

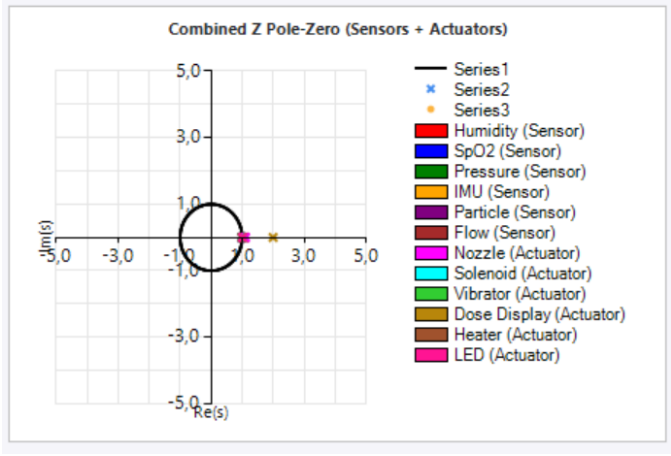

Fig. 15. z Domain Mapping Filtered Signal

TABLE I
COMPARISON OF RAW, NOISY, AND FILTERED MULTI-DOMAIN CHARACTERISTICS

Domain	**Raw Signal**	**Noisy Signal**	**Filtered Signal**
Time-domain	Periodic, smooth, stable waveform	Distorted, high-frequency jitter, reduced clarity	Restored smoothness, artefacts suppressed
FFT-domain	Clear dominant peak at inhalation freq	Broadband elevation, reduced SNR	Peak restored, noise floor reduced
s-domain (pole–zero)	Compact, well-structured distribution	Scattered, less coherent mapping	Poles/zeros reconverge to stable layout
z-domain	Tight cluster near unit circle	Widely dispersed spectral points	Compact, stable discrete-time response

filtered versions of each signal, are visualized through the developed graphical user interface. This multi-domain visualization framework demonstrated the restoration of signal integrity through IIR filtering, revealed noise-induced distortions, and effectively characterized inhalation quality. The results further highlight the system's capability to monitor subtle variations in actuator performance, particle concentration, inhalation flow, and device orientation. The modeling framework was validated using IMU-based examples, which exhibited coherence in raw signals, notable instability under noise, and recovery of dynamic consistency after filtering.

Overall, by integrating cross-domain signal analytics, actuator modulation, and real-time sensing on a single platform, this work offers an extensible foundation for intelligent inhaler design. The system enables adaptive aerosol delivery control based on physiological and environmental feedback while improving the precision of adherence assessment. Future work includes hardware prototyping, machine learning–based inhalation pattern recognition, integration with wireless health platforms, and validation through clinical studies to assess performance under real-world inhalation conditions.

ACKNOWLEDGMENT

The authors extend their appreciation for the support provided by Dwi Oktavianto Wahyu Nugroho, S.T., M.T., during the completion of this research study. His guidance and supervision offered valuable insights that enabled the successful completion of the work. The authors are also grateful to the Instrumentation Engineering Department, Faculty of Vocational Studies, Sepuluh Nopember Institute of Technology, for their collaboration and assistance, as well as for granting access to laboratory facilities for system modeling and simulation. Appreciation is also expressed to colleagues and peers who contributed feedback during the software development, simulation, and troubleshooting processes for the multi-sensor inhaler system.

REFERENCES

[1] D. M. G. Halpin and D. A. Mahler, "Systematic review of the effects of patient errors using inhaled delivery systems on clinical outcomes in COPD," *BMJ Open Respiratory Research*, vol. 11, no. 1, p. e002211, Apr. 2024, doi: 10.1136/bmjresp-2023-002211.

[2] C. Zabczyk and J. D. Blakey, "The effect of connected 'smart' inhalers on medication adherence," *Frontiers in Medical Technology*, vol. 3, Aug. 2021, doi: 10.3389/fmedt.2021.657321.

[3] D. F. Fletcher, V. Chaugule, L. G. dos Reis, P. M. Young, D. Traini, and J. Soria, "On the use of computational fluid dynamics (CFD) modelling to design improved dry powder inhalers," *Pharmaceutical Research*, vol. 38, no. 2, pp. 277–288, Feb. 2021, doi: 10.1007/s11095-020-02981-y.

[4] A. H. Y. Chan *et al.*, "Digital inhalers for asthma or chronic obstructive pulmonary disease: A scientific perspective," *Pulmonary Therapy*, vol. 7, no. 2, pp. 345–376, Dec. 2021, doi: 10.1007/s41030-021-00167-4.

[5] Y. Gao *et al.*, "Reliability and usability of a portable spirometer compared to a laboratory spirometer," *BMC Pulmonary Medicine*, vol. 25, no. 1, p. 228, May 2025, doi: 10.1186/s12890-025-03690-1.

[6] H. H. Jin, J. R. Fan, M. J. Zeng, and K. F. Cen, "Large eddy simulation of inhaled particle deposition within the human upper respiratory tract," *Journal of Aerosol Science*, vol. 38, no. 3, pp. 257–268, Mar. 2007, doi: 10.1016/j.jaerosci.2006.09.008.

[7] A. R. Martin and W. H. Finlay, "The effect of humidity on the size of particles delivered from metered-dose inhalers," *Aerosol Science and Technology*, vol. 39, no. 4, pp. 283–289, Apr. 2005, doi: 10.1080/027868290929314.

[8] V. Saroli, C. Massaroni, S. Silvestri, and E. Schena, "Advancing flow rate measurement: Innovations and challenges in spirometry and mechanical ventilation," *IEEE Sensors Reviews*, vol. 2, pp. 76–85, 2025, doi: 10.1109/SR.2025.3554130.

[9] O. Ozyurt, "Methods of classifying aerosol types by using scattering of light," in *2022 International Conference on Innovations in Intelligent Systems and Applications (INISTA)*, IEEE, Aug. 2022, pp. 1–6, doi: 10.1109/INISTA55318.2022.9894146.

[10] J. Barreiros *et al.*, "Self-sensing elastomeric membrane for haptic bubble array," in *2020 3rd IEEE International Conference on Soft Robotics (RoboSoft)*, IEEE, May 2020, pp. 229–236, doi: 10.1109/RoboSoft48309.2020.9116051.

[11] S. Takano *et al.*, "An inhalation device with inertial measurement unit for monitoring inhaler technique," *IEEE/ASME Transactions on Mechatronics*, vol. 27, no. 4, pp. 2204–2211, Aug. 2022, doi: 10.1109/TMECH.2022.3175851.

[12] Kavyashree, K. Lavanya, K. Nikitha, Sowmya, and S. R. Deepthi, "Low-cost wearable asthma monitoring system with a smart inhaler," in *2021 Asian Conference on Innovation in Technology (ASIANCON)*, IEEE, Aug. 2021, pp. 1–7, doi: 10.1109/ASIANCON51346.2021.9544970.

[13] J.-T. Lin *et al.*, "Non-invasive SpO_2 monitoring using reflective PPG: A low-cost calibration method," in *2023 International Conference on Consumer Electronics - Taiwan (ICCE-Taiwan)*, IEEE, Jul. 2023, pp. 159–160, doi: 10.1109/ICCE-Taiwan58799.2023.10226743.

[14] M. Jahed, J. Kozinski, and L. Pakzad, "The impact of actuator nozzle and surroundings condition on drug delivery using pressurized-metered dose inhalers," Apr. 2023, doi: 10.21203/rs.3.rs-2823997/v1.

[15] M. S. Hashem, J. B. Joolee, W. Hassan, and S. Jeon, "Soft pneumatic fingertip actuator incorporating a dual air chamber to generate multi-mode simultaneous tactile feedback," *Applied Sciences*, vol. 12, no. 1, p. 175, Dec. 2021, doi: 10.3390/app12010175.

[16] I. Mysovskikh, M. Legg, and S. Demidenko, "Flowrate sensing and measurement in portable smart inhalers," *Sensors*, vol. 24, no. 21, p. 6848, Oct. 2024, doi: 10.3390/s24216848.

[17] H. Chrystyn *et al.*, "Investigating the accuracy of the Digihaler ...," *Journal of Aerosol Medicine and Pulmonary Drug Delivery*, vol. 35, no. 3, pp. 166–177, Jun. 2022, doi: 10.1089/jamp.2021.0031.

[18] Z. Fan, Y. Ye, J. Chen, Y. Ma, and J. Zhu, "Development of an AI-empowered digital monitoring system for inhalation flow profiles," *Sensors*, vol. 25, no. 14, p. 4402, Jul. 2025, doi: 10.3390/s25144402.

[19] G. Dong *et al.*, "Respiratory sounds classification by fusing the time-domain and 2D spectral features," in *2024 IEEE International Conference on Bioinformatics and Biomedicine (BIBM)*, IEEE, Dec. 2024, pp. 3178–3181, doi: 10.1109/BIBM62325.2024.10822226.

[20] J. Vicente Martínez, É. Ramírez Laboreo, and P. Calderón Gil, "Modelado dinámico y control predictivo de un sistema microfluídico," *Revista Iberoamericana de Automática e Informática Industrial*, vol. 21, no. 3, pp. 231–242, Feb. 2024, doi: 10.4995/riai.2024.19953.

[21] R. Jaros *et al.*, "Multisensor fusion for noninvasive worker health monitoring in Industry 4.0," *IEEE Transactions on Instrumentation and Measurement*, vol. 74, pp. 1–15, 2025, doi: 10.1109/TIM.2025.3576005.

[22] A. K. Sen and J. Darabi, "Modeling and optimization of a microscale capacitive humidity sensor for HVAC applications," *IEEE Sensors Journal*, vol. 8, no. 4, pp. 333–340, Apr. 2008, doi: 10.1109/JSEN.2008.917479.

[23] M. Krizea *et al.*, "Accurate detection of heart rate and blood oxygen saturation in reflective photoplethysmography," in *2020 IEEE International Symposium on Signal Processing and Information Technology (ISSPIT)*, IEEE, Dec. 2020, pp. 1–4, doi: 10.1109/ISSPIT51521.2020.9408845.

[24] I. Mysovskikh, M. Legg, and S. Demidenko, "Flowrate sensing and measurement in portable smart inhalers," *Sensors*, vol. 24, no. 21, p. 6848, Oct. 2024, doi: 10.3390/s24216848.

[25] R. Buchanan *et al.*, "Deep IMU bias inference for robust visual-inertial odometry with factor graphs," *IEEE Robotics and Automation Letters*, vol. 8, no. 1, pp. 41–48, Jan. 2023, doi: 10.1109/LRA.2022.3222956.

[26] R. Zhang *et al.*, "Forward and lateral dual-angle optical particle counter data fusion to detect particle mass concentration," in *2021 IEEE 15th International Conference on Electronic Measurement & Instruments (ICEMI)*, IEEE, Oct. 2021, pp. 341–345, doi: 10.1109/ICEMI52946.2021.9679661.

[27] N. A. Rodriguez-Olivares, L. Nava-Balanzar, and L. Barriga-Rodriguez, "Differential pressure spirometry for mechanical ventilation using dichotomic search," *IEEE Transactions on Instrumentation and Measurement*, vol. 70, pp. 1–10, 2021, doi: 10.1109/TIM.2021.3116307.

[28] A.-N. Tudosie, "Aircraft jet engine exhaust nozzle controller based on turbine pressure ratio sensor with micro-jet system," in *2012 International Conference on Applied and Theoretical Electricity (ICATE)*, IEEE, Oct. 2012, pp. 1–6, doi: 10.1109/ICATE.2012.6403464.

[29] Z. Peng *et al.*, "Analysis and identification of a dynamic model for proportional solenoid," *IEEE Access*, vol. 9, pp. 92651–92660, 2021, doi: 10.1109/ACCESS.2021.3092142.
[30] R. Fan, X. Zhang, and Z. Tu, "Luminance compensation and optimization to delay OLED degradation based on equivalent lifetime detection," *IEEE Journal of the Electron Devices Society*, vol. 8, pp. 626–634, 2020, doi: 10.1109/JEDS.2020.3001657.
[31] J. Laconte, C. Dupont, D. Flandre, and J.-P. Raskin, "SOI CMOS compatible low-power microheater optimization for the fabrication of smart gas sensors," *IEEE Sensors Journal*, vol. 4, no. 5, pp. 670–680, Oct. 2004, doi: 10.1109/JSEN.2004.833516.
[32] D.-S. Shin *et al.*, "Modified diode equations for light-emitting diodes considering radiative and nonradiative currents," in *2019 34th International Technical Conference on Circuits/Systems, Computers and Communications (ITC-CSCC)*, IEEE, Jun. 2019, pp. 1–2, doi: 10.1109/ITC-CSCC.2019.8793302.
[33] J. Lu *et al.*, "Computer simulation analysis of flow noise and vibration performance for heat supply network bleed," in *2022 2nd International Conference on Computational Modeling, Simulation and Data Analysis (CMSDA)*, IEEE, Dec. 2022, pp. 120–129, doi: 10.1109/CMSDA58069.2022.00029.
[34] M. Kumar, "Design and implementation of digital low pass FIR and IIR filters using VHDL for ECG denoising," *International Journal of Engineering Trends and Technology*, vol. 72, no. 1, pp. 252–265, Jan. 2024, doi: 10.14445/22315381/IJETT-V72I1P125.
[35] R. Aisuwarya, H. Hendrick, and M. Meitiza, "Analysis of cardiac frequency on photoplethysmograph (PPG) synthesis for detecting heart rate using fast Fourier transform (FFT)," in *2019 International Conference on Electrical Engineering and Computer Science (ICECOS)*, IEEE, Oct. 2019, pp. 391–395, doi: 10.1109/ICECOS47637.2019.8984512.
[36] P. Lu and F. Dai, "An overview of multi-sensor information fusion," in *2021 6th International Conference on Intelligent Informatics and Biomedical Sciences (ICIIBMS)*, IEEE, Nov. 2021, pp. 5–9, doi: 10.1109/ICIIBMS52876.2021.9651656.
[37] F. Rezvanifard and F. Radmehr, "Laplace transform in mathematics and electrical engineering: A praxeological analysis of two textbooks on the differential equations and signal processing," *IEEE Transactions on Education*, vol. 67, no. 4, pp. 508–518, Aug. 2024, doi: 10.1109/TE.2024.3349662.
[38] A. N. Borodzhieva and S. Zaharieva, "Z-transform in the learning process: Interactive approaches for more effective digital signal processing training," in *2025 XXXIV International Scientific Conference Electronics (ET)*, IEEE, Sep. 2025, pp. 1–6, doi: 10.1109/ET66806.2025.11204126.

BIOGRAPHIES

Mahendra Dwi Fahreza studied Industrial Automation Engineering at SMK Negeri 1 Batam, graduating in 2020. He completed industrial internships as an Assistant Method Engineer at PT TESE Manufacturing Indonesia and as a Facilities Technician at PT SIIX Electronics Indonesia. He is currently pursuing a Bachelor's degree in Instrumentation Engineering at the Department of Instrumentation Engineering, Faculty of Vocational Studies, Institut Teknologi Sepuluh Nopember (ITS), starting in 2024.

His academic interests include digital systems, embedded systems, automation engineering, and cyber-physical systems. He can be contacted at the following email address: mahendrafhrz1202@gmail.com.

Ir. Dwi Oktavianto Wahyu Nugroho S.T., M.T received his Bachelor's degree in Electro Engineering from the Engineering Faculty, Brawijaya University, in 2009. He completed his Master's degree in Electrical Engineering (Industrial Electronics) at the Institut Teknologi Sepuluh Nopember (ITS) in 2016. His academic interests include medical instrumentation, sensor system development, energy harvesting, and mechatronics.

He began his professional career in 2009 at Cipta Karya, Dinas Pekerjaan Umum, East Java Province, then continued his work at Perusahaan Daerah Air Minum (PDAM) in Sidoarjo from 2010 to 2017. He currently serves as a lecturer in the Department of Instrumentation Engineering, Faculty of Vocational Studies, Institut Teknologi Sepuluh Nopember.